

# **A deep learning approach to single-particle recognition in cryo-electron microscopy**

**Yanan Zhu<sup>1</sup>, Qi Ouyang<sup>1</sup>, Youdong Mao<sup>1,2\*</sup>**

<sup>1</sup>Center for Quantitative Biology, State Key Laboratory for Mesoscopic Physics, Institute of Condensed Matter Physics, School of Physics, Peking University, Beijing 100871, China.

<sup>2</sup>Intel Parallel Computing Center for Structural Biology, Dana-Farber Cancer Institute, Department of Microbiology and Immunobiology, Harvard Medical School, Boston, MA 02115, USA.

\*Corresponding author. Tel: +1 617 632 4358. Fax: +1 617 632 4338. E-mail address: youdong\_mao@dfci.harvard.edu (Y. M.).

## **Abstract**

**Particle extraction represents a major practical bottleneck in the structure determination of biological macromolecular complexes by single-particle cryo-electron microscopy (cryo-EM). We developed a deep learning-based algorithmic framework, DeepEM, for single-particle recognition from noisy cryo-EM micrographs, enabling automated particle picking, selection and verification in an integrated fashion. Our approach exhibits improved performance and high accuracy when tested on the standard KLH dataset as well as several challenging experimental cryo-EM datasets.**

Single-particle cryo-EM images suffer from heavy background noise and low contrast, due to a limited electron dose used in imaging for reducing radiation damage to biomolecules of interest. Hence, a large number of single-particle images, extracted from cryo-EM micrographs, are required to perform reliable 3D reconstruction of the underlying structure. Particle recognition thus represents the first bottleneck in the practice of cryo-EM structure determination. During the past decades, many computational methods have been proposed for automated particle recognition. Most of these are based on template matching, edge detection, image features or neural networks. The template matching methods<sup>1,2,3,4,5,7,7</sup> depend on local cross-correlation that is sensitive to noise. A substantial fraction of false positives may result from false correlation peaks. Similarly, both the edge-based<sup>9,9</sup> and feature-based methods<sup>10,11,12</sup> suffer from a dramatically reduced performance with lowering the contrast of micrographs. A method based on a three-layer pyramidal-type artificial neural network was developed<sup>13,14</sup>. But there is only one hidden layer in the designed neural network, which is insufficient to extract rich features in single-particle images. A common problem for these automated particle recognition algorithms lies in that they cannot distinguish

“good particles” from overlapped particles, local aggregates, background noise fluctuation, ice contamination and carbon areas. Thus, additional steps by image classification or by manual selection were necessarily practiced to sort out “good particles” after initial automated particle picking. For example, TMaCS<sup>15</sup> uses support vector machine (SVM) to classify the particles initially picked by a template-matching method to remove false positives<sup>15</sup>.

Deep learning<sup>16, 32</sup> is a type of machine learning that focuses on learning multiple levels of feature representations, which help to make sense of data such as images, sound and text. It is a process of layered feature extraction; features in greater detail can be extracted with moving up the hidden layer to a deeper level using the multiple non-linear transformations<sup>32</sup>. The area of deep learning consists of deep belief networks (DBNs)<sup>17,18</sup>, convolutional neural networks (CNNs)<sup>19</sup>, recurrent neural networks (RNNs)<sup>20</sup> and any other deep networks with more than one hidden layer. CNN is a biologically inspired deep, feedforward neural network, and has demonstrated outstanding performance on speech recognition and image processing, such as handwriting recognition<sup>21</sup>, face detection<sup>22</sup> and cell image classification<sup>23</sup>. Its unique advantage<sup>31,33</sup> lies in that the special structure of the shared local weights reduces the complexity of the network. Multidimensional vector images can be directly used as inputs of the network, which avoids the complexity for the feature extraction in the reconstructed data<sup>16,31</sup>.

The particle recognition problem in cryo-EM is fundamentally a binary image classification problem based on the features of single-particle images. We devised a novel automatic particle recognition approach based on deep CNN learning. The deep CNN can be understood as a self-learning process of local particle image features from lower to higher spatial frequencies. We designed a six-layer CNN in our DeepEM (Details in Fig. 1). The first, third, and fifth layers are convolutional, in which the connections are local, but expand throughout the entire input image. This would ensure that the learnt filters

produce the strongest response to a spatially local input. The second, fourth and sixth layers are designed to subsample their input data to progressively decrease the spatial size of the representation to reduce the amount of parameters and computation in the network, and hence also to control over-fitting<sup>36</sup>. There are full connections between the sixth and the final classification output layer.

Prior to the application of DeepEM in automated particle recognition, the CNN needs to be trained with a manually assembled dataset including samplings of both particle images (positive training dataset) and non-particle images (negative training dataset) (Examples in Fig. 2a, b). We use the error back-propagation method<sup>30</sup> to train the network and produce an output of 1 for the true particle images and 0 for the non-particle images. Data augmentation technique<sup>13,23</sup> has shown improvement in accuracy for training the CNNs with a large number of parameters. During our CNN training, each training particle image is rotated by 90, 180 and 270 degrees, to augment the data sampling by four times. When a well-trained CNN is used to recognize particles, each input image boxed from a testing micrograph is also rotated in the same way as the training images. The final expectation value of each input image is taken as the average of its four output values. F-measure<sup>35</sup> is a measure on the accuracy of a test that combines both precision and recall for binary classification problems. Based on the F-measure, we determine a threshold for particle selection, at which the F-score presents a maximum value. Those particles with the expectation values below the threshold are excluded (see Methods). To further improve the accuracy of the recognition, one can optimize the training dataset by adding some true and false positive images to the original training dataset, then re-train the network (workflow chart in Supplementary Fig. 1a). After sufficient iterations of training, the CNN becomes 'knowledgeable' in differentiating positive particles from negative ones. Depending on the standard deviation of the particle images, a well-trained CNN can recognize and eliminate automatically the false positives resulting from the background noisy images,

contaminants, broken ice and carbon areas in the micrographs, even though they may result in an initially high score from the CNN.

We first tested our DeepEM algorithm on the Keyhole Limpet Hemocyanin (KLH)<sup>26</sup> dataset that was previously used as a standard testing dataset to benchmark various particle selection methods<sup>2,3,5,7,10,11,12,15</sup>. The precision-recall curve<sup>27</sup> is one of the popular metrics to evaluate the performance of different particle selection algorithms. Higher precision indicates that an algorithm selects a less percent of non-particles. Higher recall means that an algorithm selects a greater percent of the true particle images contained in the micrographs (see Methods). For the KLH dataset, the recall and the precision can both reach ~90% at the same time in the precision-recall curve (Fig. 2f) plotted against a manually selected set of particle images from 32 micrographs, which did not include any particle images used in the training dataset. Our approach achieves a higher precision over all of the particle images selected, whereas the recall is still kept at a high value, indicating that fewer false-negative particle images are missed in the micrographs. In a typical KLH micrograph (Fig. 2c), all true particle images are automatically recognized by our method with a threshold of 0.84, which is determined by the F-measure<sup>35</sup> (Fig. 2e).

We also applied our method to several challenging cryo-EM datasets collected with a direct electron detector. There are three different kinds of datasets, the 19S regulatory complex, 26S proteasome and inflammasome<sup>34</sup>. Figure 2d shows a typical micrograph of 19S, in which DeepEM avoids selecting non-particles from areas of aggregates and carbon film. The precision-recall curve resulting from the test on the 19S dataset is shown in Fig. 2f. The precision and recall can both reach ~80%. The picked particles are approximately well centered compared to the manually selected ones. To further verify that the particle images selected are correct, we performed reference-free 2D classification. The resulting unsupervised class averages from about 100 micrographs for the dataset are consistent with different views of the protein samples (Supplementary Fig.

2). Figure 3 shows two difficult examples from the inflammasome dataset. The results show that when the spatial density of the particles in a micrograph is very high or very low, DeepEM can still perform quite well in avoiding selection of overlapped particles and non-particles.

Our DeepEM algorithm framework exhibits several advantages. First, with sufficient training, DeepEM can select true particles without picking non-particles, in a single, integrative step of particle recognition. It performs as well as a human worker. The similar performance was only made possible previously through combining several steps in automated particle picking, classification and manual curation. Second, DeepEM features the traits representative of other artificial intelligent (AI) or machine learning systems. The more it is trained or learned, the better it performs. We found that with iteratively updating or optimizing the training dataset, the performance in particle recognition by DeepEM can be further improved. However, this was not possible for conventional particle-recognition algorithms developed so far, whose performance was intricately bound by their mathematics and control parameters. Finally, we expect that DeepEM marks the inception of applications of modern AI technology in expediting cryo-EM structure determination. Related AI technology may be developed in the near future to address key challenges in this area, such as deep classification of highly heterogeneous cryo-EM datasets.

## **Methods**

**Design of mathematical model .** Convolutional neural network is a kind of multilayer neural network with incomplete connections. It contains convolutional layers, subsampling layers and fully connected layers in addition to the input and output layers. The convolutional and subsampling layers produce feature maps through repeated

application of the activation function across sub-regions of the image, which represent different features extracted from the previous layer.

The convolutional layer is the core building block in a CNN, in which the feature maps from the previous layer convolute with a learnable kernel; all convolution operation outputs are then transformed by a nonlinear activation function. In the paper we use the sigmoid function as the nonlinear activation function:

$$\text{sigmoid}(x) = \frac{1}{1 + e^{-x}} \quad (1)$$

The convolution operations in the same convolutional layer would share the same connectivity weights with the previous layer:

$$X_j^l = \text{sigmoid}\left(\sum_{i \in M_j} X_i^{l-1} * W_{ij}^l + B^l\right) \quad (2)$$

where  $l$  represents the convolutional layer;  $W$  represents the shared weights;  $M$  represents different feature maps in the previous layer;  $j$  represents one of the output feature maps and  $B$  represents the bias in the layer.

Subsampling, which is a form of non-linear down-sampling, is another important concept of CNNs. We computed subsampling average after each convolutional layer using the following expression, which would reduce the spatial size of the representation.

$$X_{ij}^l = \frac{1}{MN} \sum_m^M \sum_n^N X_{iM+m, jN+n}^{l-1} \quad (3)$$

Here  $i$  and  $j$  represent the position of the output map.  $M$  and  $N$  represent the subsampling size.

The basic network architecture designed in DeepEM contains three convolutional layers and three subsampling layers. The last layer, output layer, is fully connected with the previous layer, which make predictions of the input image by a weight matrix and the activation function.

**Training of the DeepEM model.** The initial weights in the DeepEM are given by a random number between 0 and 1 and all the weights are then updated in the process of training. We use the squared-error loss function as the objective function in our model. For a training dataset with the number of  $N$ , it is defined by equation (4), in which  $t^n$  is the  $n$ -th training image's corresponding target, and  $y^n$  is similarly the value of the output layer in response to the  $n$ -th input training image.

$$E^N = \frac{1}{2N} \sum_{n=1}^N \|t^n - y^n\|^2 \quad (4)$$

During the process of training, the objective function is minimized using error back propagation algorithm<sup>30</sup> which performs a gradient-based update:

$$\omega(t+1) = \omega(t) - \frac{\eta}{N} \sum_{k=1}^N \varepsilon^n \frac{\partial \varepsilon^n}{\partial \omega} \quad (5)$$

Here  $\varepsilon^n = \|t^n - y^n\|$ ,  $\omega(t)$  and  $\omega(t+1)$  represent parameters before and after update in an iteration, respectively; and  $\eta$  is the learning rate. We set the  $\eta$  value to 1 in this study.

Since the input particle images size may vary in different datasets. We set different number of the feature maps, size of the convolutional kernel of the convolutional layers and pooling region size for pooling layers. The details of these hyper-parameters used in this study are shown in Supplementary Table 1. All of the algorithms are implemented in Matlab. We design and implement the convolutional neural network based on the DeepLearnToolbox<sup>25</sup>, which is a Matlab toolbox for Deep Learning development.

**Particle recognition and selection in the DeepEM model.** We used two criteria to select particles. First, we define a threshold score. The particle is identified as a candidate if the CNN output score of the particle is above the threshold. Those particles whose CNN scores are below the threshold are rejected. We used the F-measure<sup>35</sup> to determine



the threshold cutoff in our approach, which is defined by equation (8).

$$F_{\beta} = (1 + \beta^2) * \frac{precision*recall}{(\beta^2*precision+recall)} \quad (8)$$

where  $\beta$  is a coefficient weighting the importance of precision and recall. In our method, we use the  $F_2$  score, which weights recall higher than precision. The F-score reaches its best value at 1 and worst at 0. We define the cutoff threshold at the highest value of the F-score. Second, particle images are further selected based on the standard deviation of the pixel intensities. In brevity, we set a narrow range of the standard deviation corresponding to true particles. Those particles whose pixel standard deviations are out of the range are rejected. This step helps remove those false particle candidates in the carbon areas or contaminants (Supplementary Fig. 3).

### **DeepEM algorithm workflow.**

Learning process

Input: Training dataset

Output: Trained Convolutional Neural Network parameters (weights and bias)

1. Rotate the particle image three times, each with a 90-degree increment;
2. Set the output of the positive data as 1, the output of the negative data as 0;
3. Initialize the hyper-parameters;
4. Randomly initialize the weights and bias in each convolutional layer;
5. Training weights and bias through back-propagation algorithm;
6. Tune the hyper-parameters or optimize the training dataset by adding more representative positive and negative particles to the training dataset;
7. Repeat 4-5 until the CNN output from input testing data falls below the defined error.

Recognition Process

Input: Micrographs and trained convolutional neural network

Output: Box files of selected particles in the EMAN2 format for each micrograph

1. Extract a square of particle size starting from a corner of the input micrograph;
2. Rotate the particle image three times, each with a 90-degree increment;
3. Use the trained convolutional neural network to process the particle image, including the un-rotated and rotated version and average the resulting output score of the four particle images;
4. Repeat steps 1-3 by shifting the square region 20 pixels until the whole micrograph has been raster-scanned;
5. Select the particle images depending on their scores not only local maximum but above the threshold;
6. Further select particle images based on the standard deviation;
7. Write the coordinates of the selected particle images to the box file.

**Performance evaluation.** We evaluate the performance of the method based on the precision-recall curve. The precision and recall are defined by equations (6) and (7), respectively, where the precision represents the fraction of true positives (TP) over the total particle images selected (TP+FP) and the recall represents the fraction of true positives, or true particle images selected over all of the true particle images (TP+FN) contained in the micrographs.

$$Precision = \frac{TP}{TP+FP} \quad (6)$$

$$Recall = \frac{TP}{TP+FN} \quad (7)$$

The precision-recall curve is generated from the algorithm by varying the threshold, which could be a score in the machine learning algorithms or the correlation value in the algorithms based on cross correlation. A candidate particle would be accepted as a particle image when the score reaches the threshold. With increasing the threshold, the

precision would increase and the recall would decrease normally. Thus, the threshold is manifested as a balance between the precision and the recall. For a good performance in a particle selection method, both the precision and the recall are expected to achieve a high value at a certain threshold.

**DeepEM training on the KLH dataset.** The KLH dataset are acquired from the National Resource for Automated Molecular Microscopy (nramm.scripps.edu). KLH is ~8 MDa with dimensions of ~300 x 300 x 400 Å. It consists of 82 micrographs at 2.2 Å/pixel that were acquired on a Philips CM200 microscope at 120 kV. The size of the micrograph is 2048 x 2048. There are mainly two types of projection views of the KLH complex, the side view and the top view. We boxed the particle image size with a dimension of 272 pixels. 800 particle images were manually selected for a positive training dataset; 800 randomly selected non-particle images were used as a negative dataset from the first fifty micrographs (Fig. 2a). Each image in the training dataset was rotated at 90 degree increments to create four images. We then have 3200 positive particle images and 3200 negative particle images in the training dataset. We also selected some particle images as a testing dataset, which contains some positive data as well as some negative data. The accuracy or error of CNN learning output from the test dataset was used as a feedback to tune the hyper-parameters, including the number of the feature maps, the kernel size for the convolutional layers and subsampling size for the subsampling layers in the network. For the training process, the density of each pixel of an input image was input into a neuron in the input layer; and the desired output was set to 1 for the positive particle image and to 0 for the negative data. Then we used the back-propagation algorithm to train the network. During the training process, we tuned the hyper-parameters or updated the training dataset until the accuracy of the CNN learning reaches a satisfying level. The acceptable value is often set as ~95% at the

threshold at 0.5 (Supplementary Fig.1a).

**Application to experimental cryo-EM data.** The pixel sizes of micrograph data from the inflammasome, 19S regulatory particle and proteasome holoenzyme are 0.86, 0.98 and 1.72 Å/pixel, respectively. For the inflammasome and 19S, the micrographs were binned for 4 times. Therefore, the pixel sizes we used for inflammasomes and 19S proteasomes are 3.44 and 3.92 Å/pixel, respectively. For the proteasome holoenzyme, the micrographs were binned for 2 times, resulting in the pixel size of 3.44 Å/pixel. The sizes of the micrographs are all 1855 x 1919 and the particle image sizes we used are 112, 160 and 150 pixels, respectively. These three experimental cryo-EM datasets were all acquired from an FEI Tecnai Arctica microscope equipped with a Gatan K2 Summit direct electron detector at 200 kV. We applied the DeepEM to these three challenging cryo-EM datasets. The hyper-parameters we tuned for these dataset are shown in Supplementary Table 1. Different from the training for the KLH dataset, we added the false positive and true positive data to optimize the training dataset and train the network again for the low-contrast of these datasets (Supplementary Fig. 4).

## **Acknowledgements**

The authors thank J. Wu, S. Chen, D. Yu, Y. Wang, M. Lin and H. Liu for helpful discussion. The cryo-EM experiments were performed in part at the Center for Nanoscale Systems at Harvard University, a member of the National Nanotechnology Infrastructure Network (NNIN), which is supported by the National Science Foundation under NSF award no. ECS-0335765. This work was funded by a grant of the Thousand Talents Plan of China (Y.M.), by a grant from National Natural Science Foundation of China 91530321 (Y.M., Q.O.), by the Intel Parallel Computing Center program (Y.M.), and by gifts from Mr. and Mrs. Daniel J. Sullivan, Jr..

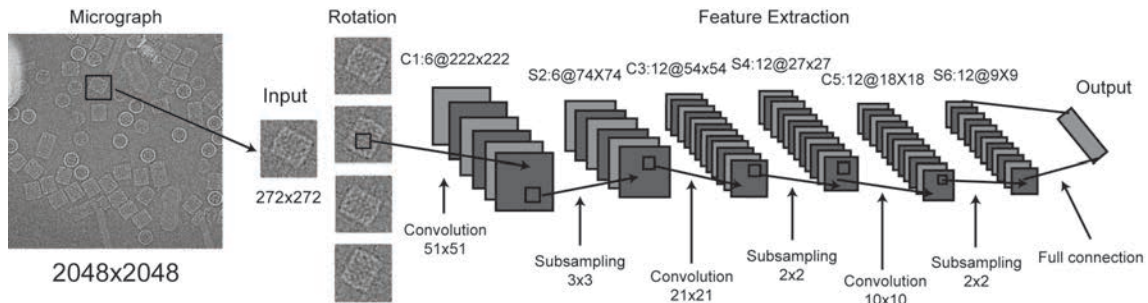


**Figure 1.** The architecture of the convolutional neural network designed in our method, in which the convolutional layer and the subsampling layer are abbreviated as C and S. C1:6@222×222 means that this is a convolutional layer and is the first layer of the network. This layer is comprised of six feature maps, each of which has a size of 222 × 222. The symbols and number above the feature maps of other layers have the similar meaning.

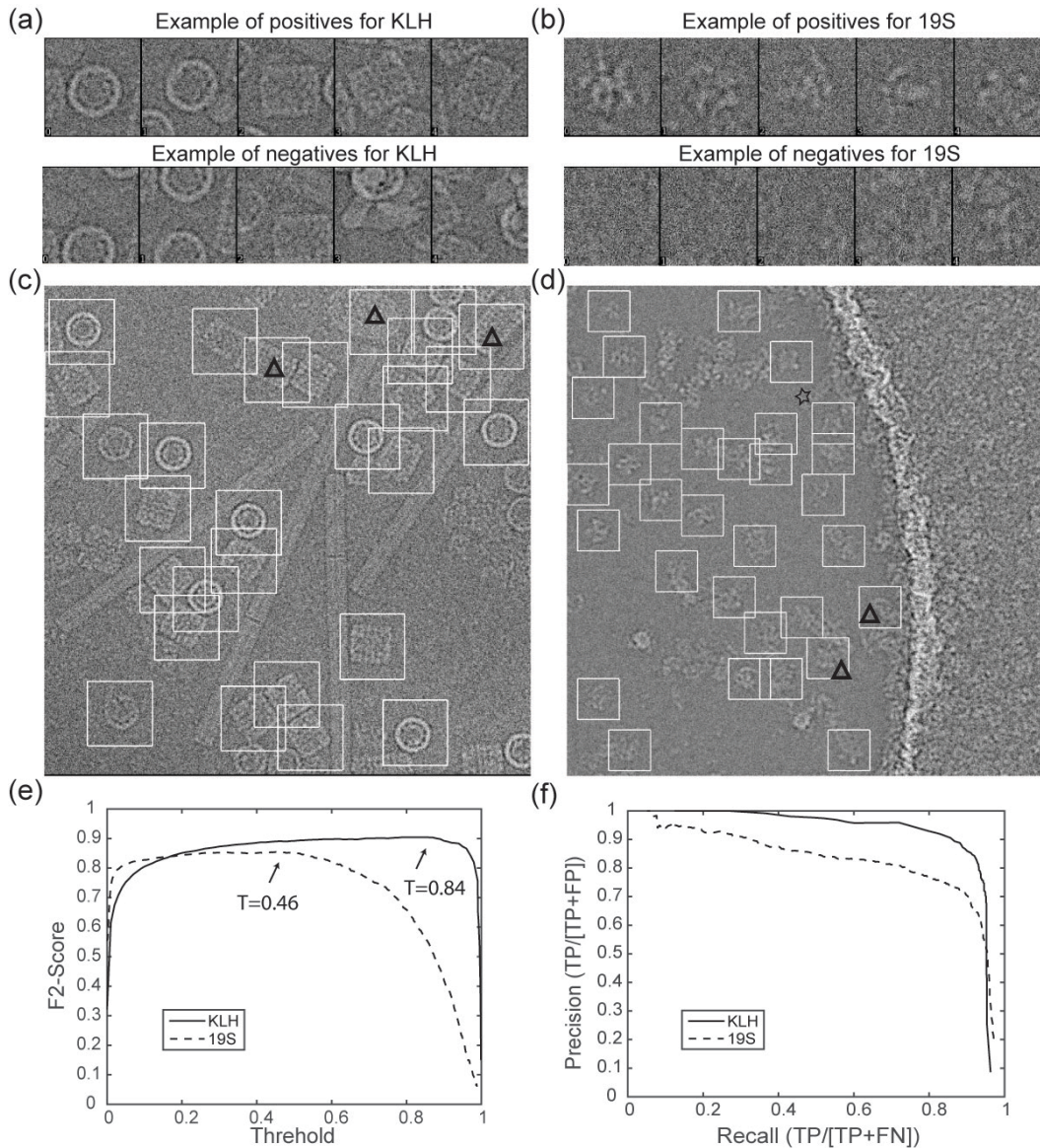


**Figure 2.** The DeepEM results of KLH dataset and 19S regulatory particles. (a) and (b) The example of positive and negative particle images selected previous respectively. (c) and (d) Typical micrographs from KLH dataset in which the white square boxes indicate the positive particle images we selected and boxes with a triangle in them indicate that the false-positive particle images picked. (e) The  $F_2$ -score curves through different threshold, the arrows indicate the peak in each curve and we select the cutoff threshold value there. (f) The precision recall curves constructed against previous manually selected list of particle images.

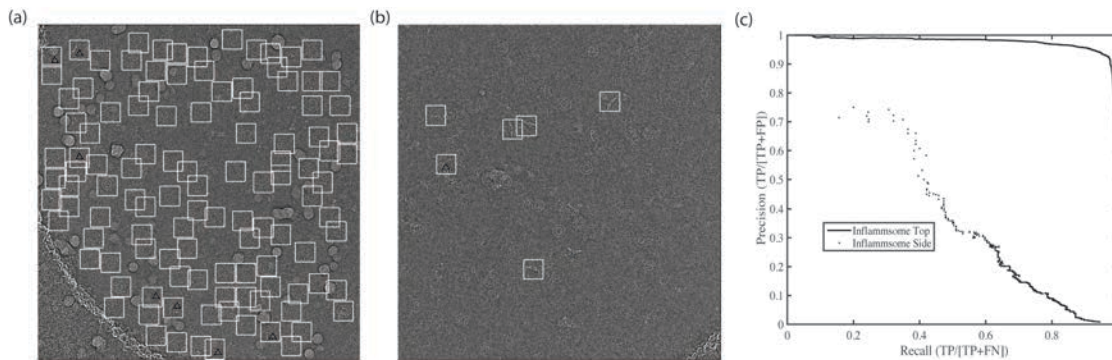


**Figure 3.** Two challenging examples of automated particle recognition. (a) A typical example of high density top view of the inflammasome complex. (b) A typical example of side view showing both few features and a low density of objects. The white square boxes indicate the positive particle images selected by DeepEM. Boxes with a triangle inside indicate that the false-positive particle images picked. Boxes with a star inside indicate the particle images left. (c) The precision-recall curves corresponding to the cases shown in (a) and (b).

## References

1. Roseman, A M. Particle finding in electron micrographs using a fast local correlation algorithm. *Ultramicroscopy*. 94. 225-236 (2003).
2. Huang, Z. *et al.* Application of template matching technique to particle detection in electron micrographs. *J. Struct. Biol.* 145, 29-40 (2004)
3. Roseman, A M. FindEM- a fast, efficient program for automatic selection of particles from micrographs. *J. Struct. Biol.* 145, 91-99 (2004)
4. Rath, B. K., Frank, J. Fast automatic particle picking from cryo-electron micrographs using a locally normalized cross-correlation function: a case study. *J. Struct. Biol.* 145, 84-90 (2004)
5. Grigorieff, N. *et al.* SIGNATURE: A single-particle selection system for molecular

- electron microscopy. *J. Struct. Biol.* 157, 168-173 (2007)
6. Langlois, R., *et al.* Automated particle picking for low-contrast macromolecules in cryo-electron microscopy. *J. Struct. Biol.* 186, 1-7 (2014)
  7. Scheres, S. RELION: Implementation of a Bayesian approach to cryo-EM structure determination. *J. Struct. Biol.*, 180, 519-530 (2015)
  8. Adiga, U. *et al.* Particle picking by segmentation: A comparative study with SPIDER-based manual particle picking. *J. Struct. Biol.* 152,211-220 (2005)
  9. Woolford, D. *et al.* SwarmPS: Rapid, semi-automated single particle selection software. *J. Struct. Biol.* 157, 174-188 (2007)
  10. Yu, Z. *et al.* Detecting circular and rectangular particles based on geometric feature detection in electron micrographs. *J. Struct. Biol.* 145, 168-180 (2004)
  11. Mallick, S. P. *et al.* Detecting particles in cryo-EM micrographs using learned features. *J. Struct. Biol.* 145, 52-62 (2004)
  12. Sorzano, C.O.S. *et al.* Automatic particle selection from electron micrographs using machine learning techniques. *J. Struct. Biol.* 167, 252-260 (2009)
  13. Ogura, T., Sato, C., An Automatic particle pickup method using a neural network applicable to low-contrast electron micrographs. *J. Struct. Biol.* 136, 227-238 (2001).
  14. Ogura, T., Sato, C., Automatic particle pickup method using a neural network has high accuracy by applying an initial weight derived from eigenimages: a new reference free method for single-particle analysis. *J. Struct. Biol.* 145, 63-75 (2004).
  15. Zhao, J., *et al.* TMaCS: A hybrid template matching and classification system for partially-automated particle selection. *J. Struct. Biol.* 181, 234-242 (2013)
  16. Lecun, Y., *et al.* Deep Learning. *Nature.* 521, 436-444 (2015)
  17. Hinton, G. E., *et al.* Reducing the dimensionality of data with Neural Networks. *Science.* VOL313, 504-507 (2006)



18. Hinton, G. E., et al. A fast learning algorithm for deep belief nets. 18, 1527-1554 (2006)
19. LeCun, Y. et al. Handwritten digit recognition with a back-propagation network. In Proc. Advances in Neural Information Processing Systems 396-404 (1990)
20. Medsker, L. R. et al. Recurrent neural networks design and application. CRC Press (2001)
21. Semard, D., et al. Best practices for convolutional neural network. *In Proc. Document Analysis and Recognition*. 985-963 (2003)
22. Lawrence, S. et al. Face recognition: a convolutional neural-network approach. *IEEE Trans. Neural networks*. 8 98-113 (1997)
23. Gao, Z. et al. HEP-2 cell image classification with deep convolutional neural networks. *IEEE Journal of Biomedical and Health Informatics*. (2016)
24. Waibel, A., et al. Phoneme recognition using time-delay neural network. *IEEE Trans. Acoustics Speech Signal Process*. 37, 328-339 (1989)
25. Palm, R. Prediction as a candidate for learning deep hierarchical models of data. IMM2012-06284 (2012)
26. Zhu, Y., et al. Automatic particle detection through efficient Hough transforms. *IEEE Trans. Med. Imaging* 22, 1053-1062 (2003)
27. Langlois, R. et al. A clarification of the terms used in comparing semi-automated particle selection algorithms in Cryo-EM. *J. Struct. Biol.* 175, 348-352 (2011)
28. Scheres, S. Semi-automated selection of cryo-EM particles in RELION-1.3. *J. Struct. Biol.*, 189, 114-122 (2015)
29. Tang, G. et al. EMAN2: an extensible image processing suite for electron microscopy. *J. Struct. Biol.*, 157(1), 38-46 (2007)
30. D. E. Rumelhart. et al. Learning representations by back-propagating errors. *Nature* 323, 533-536 (1986)

31. Krizhevsky A. *et al.* ImageNet classification with deep convolutional neural networks. *In Proc. 26<sup>th</sup> Annual Conf. on Neural Information Processing Systems*, 1090-1098. (2012)
32. Deng, L. *et al.* Deep learning: Methods and Applications. *Foundations and Trends in Signal Processing*. Vol.7, Nos. 3-4 197-387 (2013)
33. Mallats, S. Understanding deep convolutional networks. *Phil. Trans. R. Soc. A* 374:20150203. (2016)
34. Zhang, L. *et al.* Cryo-EM structure of the activated NAIP2-NLRC4 inflammasome reveals nucleated polymerization. *Science*. Vol. 350, Issue 6259, 404-409 (2015)
35. Powers, D.M.W. Evaluation: from precision, recall and F-measure to ROC, informedness, markedness & correlation. *Journal of Machine Learning Technologies*. 2 (1), 37-63 (2011)
36. Andrew Ng. *et al.* Feature extraction using convolution. <http://ufldl.stanford.edu/tutorial/supervised/FeatureExtractionUsingConvolution/>. (2015)